Applied Catalysis B: Environmental 115–116 (2012) 269–275

Contents lists available at SciVerse ScienceDirect

Applied Catalysis B: Environmental

journal homepage: www.elsevier.com/locate/apcatb

Enhanced oxygen reduction activity and durability of Pt catalysts supported on carbon nanofibers

David Sebastián[a], Andrés García Ruíz[a], Isabel Suelves[a], Rafael Moliner[a], María Jesús Lázaro[a,*], Vincenzo Baglio[b,1], Alessandro Stassi[b,1], Antonino Salvatore Aricò[b,1]

[a] Instituto de Carboquímica, CSIC, Miguel Luesma Castán 4, 50018, Zaragoza, Spain
[b] Istituto di Tecnologie Avanzate per l'Energia "Nicola Giordano", CNR, Via Salita S. Lucia Sopra Contesse 5, Messina, Italy

ARTICLE INFO

Article history:
Received 16 November 2011
Received in revised form
22 December 2011
Accepted 27 December 2011
Available online 31 December 2011

Keywords:
Pt catalyst
Carbon nanofibers
Fuel cell
Oxygen reduction
Durability

ABSTRACT

Carbon nanofibers (CNF) characterized by different mean diameter, BET surface area and graphicity were prepared and used as supports to enhance Pt dispersion in low temperature fuel cell catalyst. As a comparison, a conventional Pt on carbon black (Vulcan XC72R) catalyst was prepared using the same procedure. The most appropriate Pt dispersion was achieved for the carbon nanofiber support showing the best compromise in terms of BET surface area and graphicity. This catalyst shows enhanced electrochemical active surface area (ECSA) and performance for the oxygen reduction reaction (ORR) with respect to the Pt/Vulcan catalyst. A cross-analysis of the supports physical-chemical properties, ECSA and mass activity for the ORR suggests that both Pt dispersion and electronic properties as determined by the effect of surface groups and graphicity play a significant role in determining the electrocatalytic activity. Whereas, regarding the decay associated to the corrosion in accelerated degradation tests (ADT), two mitigation effects are envisaged, anchoring effect of surface groups stabilizes Pt nanoparticles with respect to dissolution, whereas a high surface graphicity index reduces carbon corrosion which acts as support for the Pt particles.

1. Introduction

During last years, a large progress has been obtained in the research and development of polymer electrolyte membrane fuel cells (PEMFC) and direct alcohol (methanol or ethanol) fuel cells regarding membranes, catalysts, bipolar plate materials and system design [1–5]. However, this progress is still not enough to fulfill the cost and durability targets for their large-scale commercialization. A critical research area concerns the electrocatalytic processes in the so-called membrane electrode assembly (MEA). For an adequate performance, platinum-based electrocatalysts are needed with a consequent high cost of the system. Several approaches to minimize Pt loading are currently under investigation, e.g. tuning the shape of nanoparticles, partial substitution of Pt by other cheaper precious and non-precious metals and use of new supports (based on carbonaceous or metal oxide compounds). The aim is to reduce electrode cost while maintaining a suitable performance [6–15]. Moreover, apart from cost, durability is a very important factor for the commercialization of polymer electrolyte fuel cells. Several phenomena can reduce the useful life of a PEM fuel cell, including platinum particle sintering and dissolution, carbon support corrosion or membrane thinning [16–20].

Carbon supports, and specifically carbon blacks (Vulcan XC72R), are commonly used to increase the metallic surface area and maximize platinum use. The performance and durability of low-temperature fuel cell electrocatalysts are strongly affected by the properties of the catalyst support. Yet, it is now widely accepted that the corrosion of carbonaceous support materials is the main cause of performance degradation of low-temperature fuel cells [21], in particular under high-potential operating conditions, in the presence of starvation effects, during prolonged maintenance in open circuit potential (OCV) or under repeated start–stop cycles [16,22,23]. To improve the stability of the carbon black supports, materials with a higher graphitic character such as carbon nanotubes and carbon nanofibers (CNFs) have been proposed for fuel cells [24–29]. Yet, limited attention was devoted to the investigation of their corrosion behavior under accelerated degradation tests. These nanostructured carbons are expected to show a lower intrinsic corrosion rate due to their highly graphitic character; however, they do not prevent carbon oxidation. Moreover, their particular crystalline structure modifies the electronic properties of the supported metal phase, leading to an increase of the electrocatalytic specific activity, and their external porous structure favors the diffusion of fluids through the electrodes, resulting in a global increase of performance. In this work, various highly

* Corresponding author. Tel.: +34 976733977; fax: +34 976733318.
E-mail address: mlazaro@icb.csic.es (M.J. Lázaro).
[1] Tel: +39 090 624237; fax: +39 090 624247.

0926-3373/$ – see front matter © 2011 Elsevier B.V. All rights reserved.
doi:10.1016/j.apcatb.2011.12.041

crystalline carbon nanofibers were in-house prepared as electrocatalyst supports and the influence of their properties on the electrochemical behavior of CNF-supported Pt catalysts subjected to accelerated degradation tests was analyzed.

2. Experimental details

2.1. Carbon nanofiber-supported platinum synthesis and characterization

In-house synthesized carbon nanofibers with diverse physical-chemical properties were used to evaluate their influence on the supported catalysts electrochemical behavior. Their synthesis procedure is reported elsewhere [30]. Basically, three synthesis temperatures were selected: 550 °C (CNF550), 650 °C (CNF650) and 700 °C (CNF700) to achieve different graphitization degrees and different porous structures according to previous works [30,31]. The growth of nanofibers was carried out for enough reaction durations to obtain a volumetric carbon content of 99%, monitoring the process by gas chromatography. It is known that synthesis at temperatures lower than 550 °C leads to very low methane conversion, and consequently very low carbon nanofibers growth rate for practical purposes, whereas synthesis at temperatures higher than 700 °C does not significantly improve crystallinity neither porosity of the nanofilaments, so the selected interval seems to be ideal in terms of the study of the support.

Platinum supported on carbon nanofibers was synthesized by a water in oil microemulsion route [32]. The composition of the microemulsion and the preparation method have been adapted and optimized in order to obtain higher electrochemical surface areas than in previous works [33]. Briefly, it consists on the preparation of a microemulsion composed by 16.5% surfactant (polyethylene glycol dodecyl ether, Brij®30, Sigma–Aldrich), 3.9% aqueous solution containing the platinum precursor (0.05 M H_2PtCl_6) and 79.6% n-heptane as the hydrophobic phase. Subsequently, the appropriate amount of support is dispersed in the microemulsion under sonication to achieve a metal concentration in the catalyst of 20 wt.%. The reduction step involves the slow addition of sodium borohydride in excess and finally the catalyst is thoroughly washed with ethanol and water to remove the chemicals used during the synthesis, and dried overnight at 60 °C.

High-resolution transmission electron microscope (HRTEM) micrographs for the carbon nanofibers and the catalyst samples were obtained using a JEOL-2000 FXII microscope at 200 kV and a spatial resolution of 0.28 nm. To obtain the micrographs, the catalyst samples were finely grinded and ultrasonically dispersed in ethanol. A drop of the resultant dispersion was deposited and dried onto a standard copper grid coated with Lacey carbon.

The crystallinity of CNFs as well as platinum crystallites was studied by X-ray diffraction. XRD patterns were performed using a Bruker AXS D8 Advance diffractometer, using Cu-Kα radiation. Crystallite sizes were calculated from the Scherrer's equation on the (0 0 2) peak for carbon and (2 2 0) peak for platinum.

Raman spectra of CNFs were obtained using a Horiba Jobin Yvon HR800 UV, using the green line of an argon laser (λ = 514.53 nm) as excitation source. The carbon ordering degree was evaluated by means of the relative intensities of D (ca. 1350 cm^{-1}) and G (ca. 1590 cm^{-1}) peaks, and the crystal size in a-axis was calculated by means of Tuinstra–Koenig equation.

Textural properties of carbon supports such as specific surface area and pore volume were calculated from nitrogen adsorption–desorption isotherms, measured at −196 °C using a Micromeritics ASAP 2020. Total surface area and pore volume were determined using the Brunauer–Emmett–Teller (BET) equation and the single point method, respectively.

Electrical conductivity measurements were performed pressing the carbonaceous powder at 10 MPa as described elsewhere [34]. The electrical resistance was measured applying electrical currents up to 0.02 A.

Energy dispersive X-ray (EDX) analyses and thermogravimetric analyses (TGA) in air were performed to quantify the metal loading in the Pt/CNF electrocatalysts. An EDX analyzer Röntec XFlash Si(Li) coupled to a Hitachi S-3400N scanning electron microscope (SEM) was used. For TGA experiments in air, a Setaram Setsys Evolution thermogravimetric analyzer was used at atmospheric pressure, the temperature was varied from room temperature to 950 °C with a rate of 5 °C min^{-1}.

2.2. Electrochemical experiments

Gas diffusion electrodes were prepared according to a procedure described elsewhere [35], consisting of carbon cloth backing, gas diffusion layer and the catalytic layer under study. To reduce the flooding effects in the sulfuric acid half-cell, a hydrophobic backing layer was used (LT 1200W ELAT, E-TEK). The catalytic layer was composed of 33 wt.% Nafion® ionomer and 67 wt.% catalyst, with a Pt loading of ca. 0.15 mg cm^{-2} (±0.01 mg cm^{-2}).

Half-cell tests were carried out in a conventional thermostated three-electrode cell consisting on the gas diffusion electrode to be tested (working electrode), a mercury-mercurous sulfate reference electrode ($Hg/HgSO_4$, sat.) and a high surface coiled platinum wire as counter electrode. The electrode geometric area was 0.2 cm^2, and a 0.5 M H_2SO_4 aqueous solution was employed as electrolyte. Gas (nitrogen or oxygen) was fed to the electrode backing layer during the tests. A μAutolab Metrohm potentionstat/galvanostat was used to perform the measurements.

Among the various methods reported in literature [16], an accelerated stress test has been selected for the evaluation of the catalysts resistance to degradation. It consists on a continuous potential cycling between 0.6 and 1.2 V vs. RHE up to a total of 1000 cycles, feeding nitrogen to the electrode. The evaluation of the decay process was carried out by in situ electrochemical tests: cyclic voltamperometry (from 0.02 to 1.2 V vs. RHE) in nitrogen and polarization curves in pure oxygen.

3. Results and discussion

The carbon nanofibers used in this work differ in their structural and morphology properties due to their different growth temperature during the synthesis process. Table 1 summarizes some basic properties of the studied supports, including carbon BET surface

Table 1
Supports physical-chemical properties.

Support	S_{BET} (m^2 g^{-1})	Pore vol. (cm^3 g^{-1})	L_c (nm)	L_a (nm)	c/2 (nm)	I_D/I_G	Elec. Cond. (S cm^{-1})[a]
CNF550	183	0.53	6.0	<2	0.337	2.39	2.7
CNF650	113	0.32	8.7	2.9	0.336	1.53	4.4
CNF700	97	0.21	9.5	5.0	0.336	0.87	13.0
Vulcan	224	0.40	2.0	3.0	0.357	1.48	8.9

[a] Measured at a compaction pressure of 10 MPa.

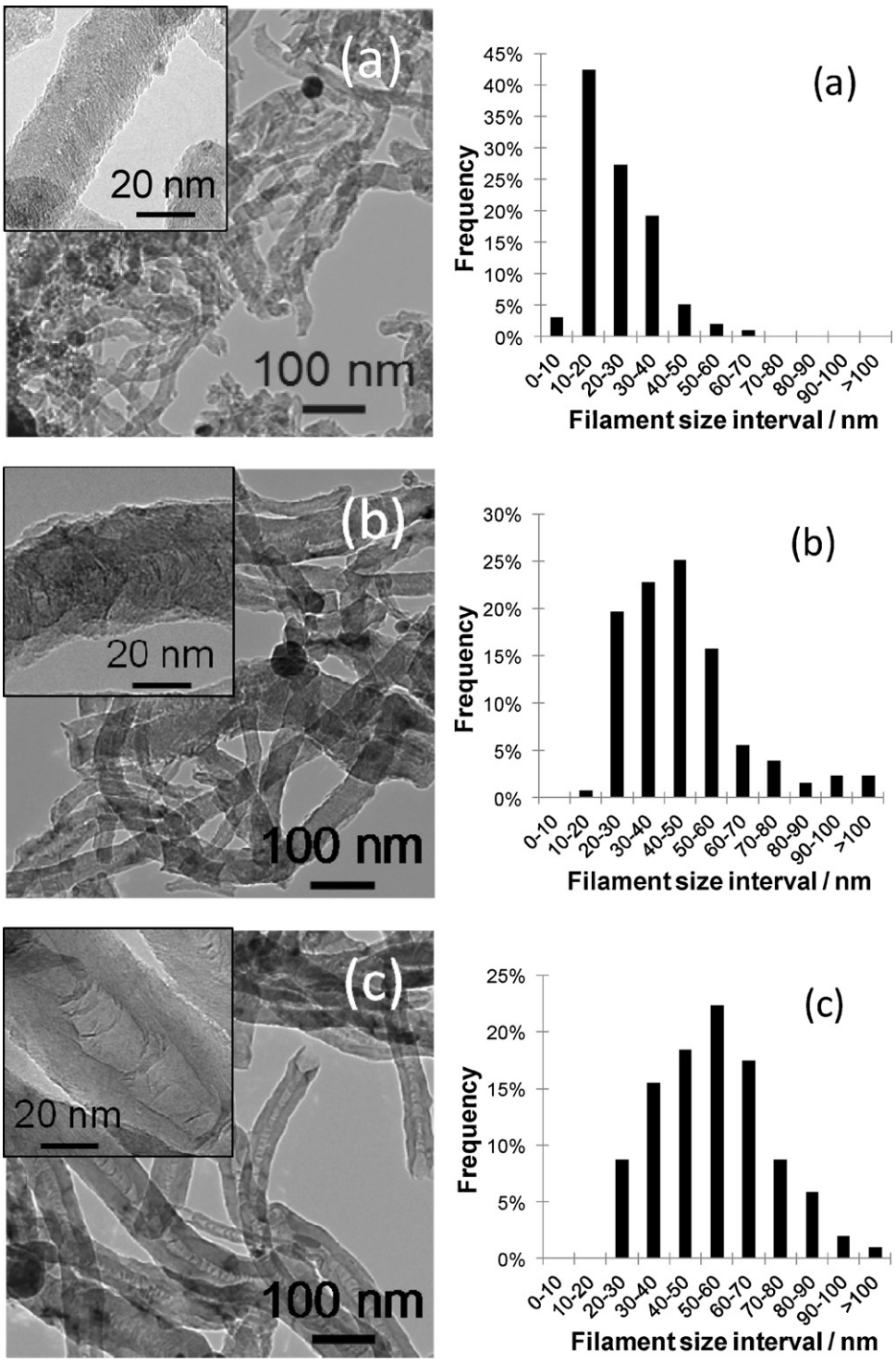

Fig. 1. TEM micrographs (inset image was captured at high magnification) and filament size distribution of (a) CNF synthesized at 550 °C; (b) CNF synthesized at 650 °C; and (c) CNF synthesized at 700 °C.

area (S_{BET}), pore volume (Pore vol.) crystal size along c-axis (L_c) and a-axis (L_a), graphenic interlayer distance (c/2), Raman intensity ratio between disorder and graphitic peaks (I_D/I_G) and electronic conductivity (Elec. Cond.). TGA and ICP-OES analyses revealed the presence of Ni, Cu and Al traces in the as prepared CNF samples due to the precursor catalyst. These elements were removed after treating them in sulfuric acid (0.5 M) at 80 °C, washing and filtering procedures. CNF synthesis temperature influences carbon characteristics in two different ways. On the one hand, a low temperature allows the catalytic growth of thin filaments because no significant sintering effects on the catalyst ($NiCuAl_2O_3$) are present; consequently, high surface area is obtained (185 $m^2\,g^{-1}$) compared to CNF synthesized at higher temperatures with a two-fold lower surface area (97 $m^2\,g^{-1}$). Moreover, the pore volume of the nanofibers varies in the same way, decreasing from 0.53 $cm^3\,g^{-1}$ (CNF synthesis at 550 °C) to 0.21 $cm^3\,g^{-1}$ (synthesis at 700 °C). These differences in porosity may influence the diffusivity of reactants and products through the catalytic layer of a fuel cell. It is important to notice that only synthesizing CNF at low temperature allows similar porosity features than the commercial carbon black (Vulcan). On the other

hand, increasing synthesis temperature favors the growth of highly ordered carbon nanofibers, as represented by the increase of crystal size, slight decrease of interlayer distance, decrease of defects (I_D/I_G ratio) and increase of electronic conductivity (Table 1). Carbon crystal size ranges from 6.0 nm to 9.5 nm in c-axis (perpendicular to graphenes) and up to 5.0 nm in a-axis (parallel to graphenes) for carbon nanofiber samples. These values are considerably higher than that of commercial carbon black (Vulcan), with 2.0 nm and 3.0 nm, respectively.

Representative TEM images of the various carbon nanofibers are collected in Fig. 1, together with the filament diameter distributions. Notice that CNFs present a relatively wide size distribution with an average that increases from ca. 25 nm to ca. 55 nm as the synthesis temperature increases. At 700 °C it is also important to notice the different structure in which a hollow cavity appears in the inner nanofilaments (Fig. 1(c)), in contrast with solid nanofilaments found at low temperatures (Fig. 1(a) and (b)). A commercial carbon black (Vulcan), Vulcan XC72R, which is the state of the art carbon used as electrocatalyst support, has been included for comparison. The BET value for Vulcan is slightly lower than that reported in the literature [36] that may be due to the fact that the sample was evacuated at relatively low temperature (150 °C) before nitrogen adsorption–desorption isotherms. An important difference regarding carbon black is the lower crystallinity of carbon, as shown by the higher interlayer distance (c/2) and lower crystallite sizes (L_c and L_a) compared to CNFs (Table 1).

Electrochemical carbon corrosion experiments were conducted in the half-cell system by means of potential holding (1.2 V vs. RHE) and using carbon coated electrodes with the same composition as the catalytic layer in the platinum catalysts electrodes, this is, a carbon loading of ca. 0.6 $mg_C\ cm^{-2}$ and the corresponding 33 wt.% Nafion loading in the carbon layer, in order to establish the carbon resistance to corrosion under same operating conditions of fuel cell catalysts. Fig. 2 represents the current–time curves for the three carbon materials studied.

Carbon electrochemical corrosion at elevated potentials proceeds through the following reaction [37]:

$$C + 2H_2O \rightarrow CO_2 + 4H^+ + 4e^- \quad (\varphi_{00} = 0.207\ V\ vs.\ RHE)$$

and the following reaction rate equation is generally accepted to describe the current–time behavior [38]:

$$j = kt^{-n}$$

The fitting parameters k and n for these current–time curves to this equation for each carbon material are summarized in Table 2.

From the log I vs. log t plot, it is clearly observed that the supports characterized by the highest corrosion rate are the CNF synthesized at 550 °C and Vulcan, whereas CNFs obtained at higher temperatures (CNF650 and CNF700) show a significant reduction of corrosion rate as also confirmed by lowest kinetic parameters, k and n (see Table 2) for the degradation process.

Platinum nanoparticles were deposited on the various supports by a microemulsion method. EDX and TGA measurements confirmed that platinum concentration was in all catalysts 20 ± 1 wt.%. The electrocatalysts XRD patterns are shown in Fig. 3, where the

Table 2
Carbon corrosion parameters.

Support	Charge [a] ($C\ g_C^{-1}$)	k ($A\ g_C^{-1}\ s^{-n}$)	n
CNF550	105	3.0	0.78
CNF650	45	1.1	0.71
CNF700	51	1.3	0.72
Vulcan	106	2.9	0.78

[a] In the time interval 0–90 min.

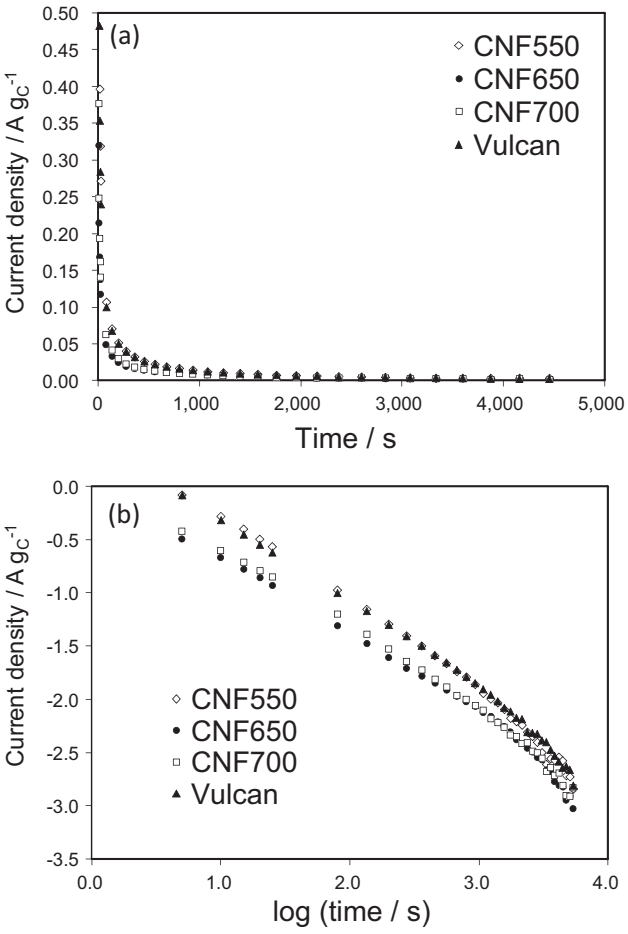

Fig. 2. Current density–time curves of carbon samples corrosion in (a) normal and (b) double logarithmic scales, performed in half-cell at 1.2 V vs. RHE, fed with nitrogen and at room temperature.

typical cubic structure (fcc) of platinum, and the hexagonal structure of graphitic carbon are observed. The mean crystallite size derived from XRD peak broadening was similar for all CNF-based catalysts (i.e. 3.5 nm), and slightly lower in Vulcan-based catalyst (3.0 nm). Representative TEM images in Fig. 4 show the most

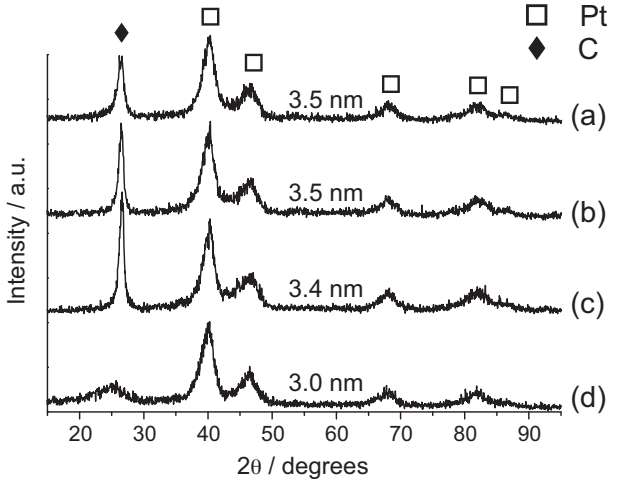

Fig. 3. XRD patterns of platinum electrocatalysts, (a) Pt/CNF550; (b) Pt/CNF650; (c) Pt/CNF700; and (d) Pt/Vulcan. The Pt crystal size is indicated for each catalyst.

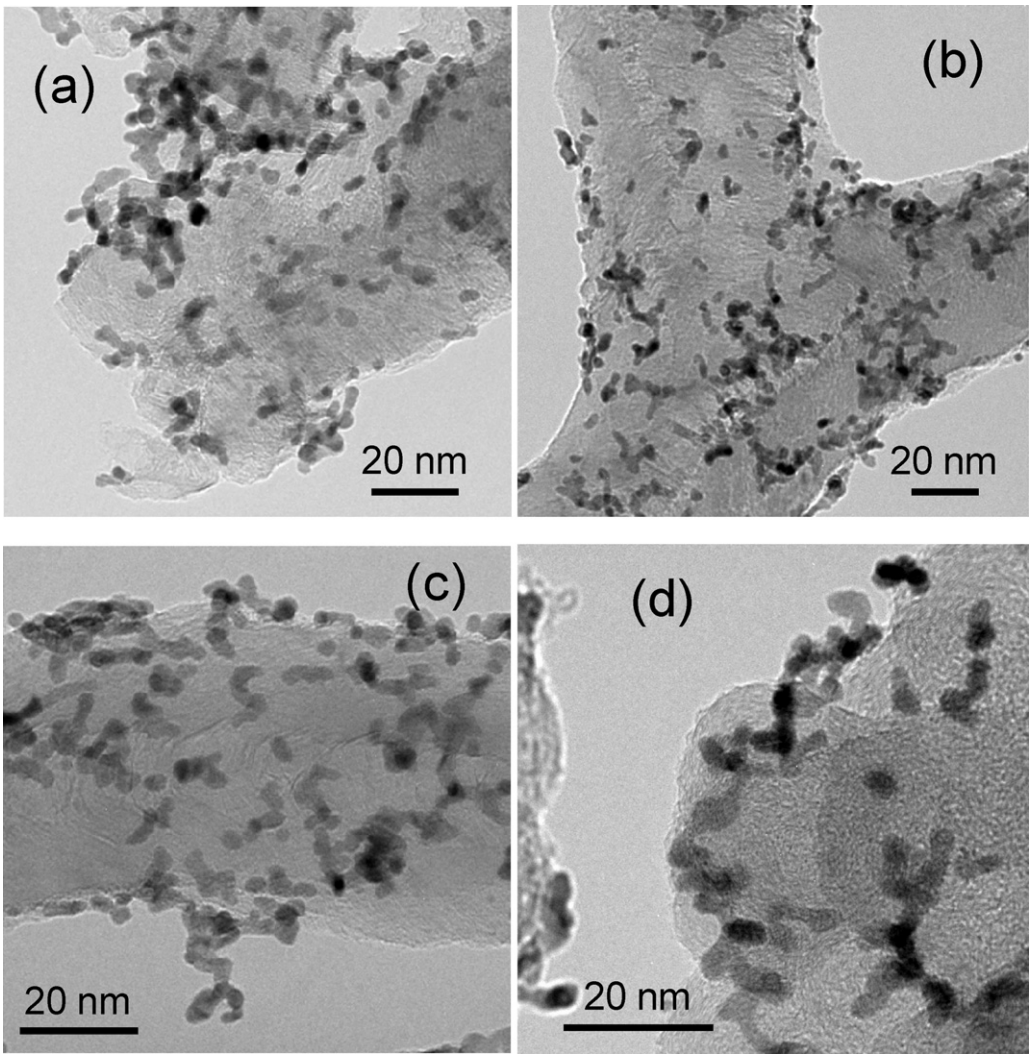

Fig. 4. Representative TEM micrographs of the different electrocatalysts, (a) Pt/CNF550; (b) Pt/CNF650; (c) Pt/CNF700; and (d) Pt/Vulcan.

appropriate distribution for the sample based on the CNF synthesized at 650 °C, being characterized by a lower degree of agglomerates with respect to the CNFs synthesized at lower and at higher temperatures. Indeed, the largest degree of agglomerates was observed for the sample based on the CNF synthesized at 550 °C despite the high surface area of the support. This appears to be related to an enhanced Pt deposition rate in the regions where a large number of defects (e.g. surface roughness) occurs. Such evidence clearly indicates that the surface characteristics, e.g. surface groups or surface roughness, govern the formation of metal particle agglomerates. In the case of the catalyst based on the CNF synthesized at 700 °C, the surface groups and surface roughness is strongly reduced (see Fig. 1) by the effect of the high synthesis temperature. Yet, there is also a decrease of BET surface area (see Table 1), as a consequence of the thicker nanofilaments which reduces the dispersion and slightly increases the surface groups content (the oxygen percentage increases from 1.5 wt.% in CNF700 to 2.6 wt.% CNF550), as reported elsewhere [34]. The best compromise in terms of catalyst morphology is thus obtained for the sample based on the CNF synthesized at 650 °C (Fig. 4).

Regarding Vulcan, the BET surface area is the highest among the various samples, but being this sample a carbon black, the concentration of surface groups and amorphous regions is considerably higher than in the CNFs (see XRD analyses). The dispersion of Pt on Vulcan does not appear better than in CNFs (Fig. 4). The electrochemically active surface area is not only determined by the particle size and the degree of dispersion but also by the interaction of Pt nanoparticles with the support surface groups. The latter may play a major role in governing the effective number of Pt sites available for the electrochemical processes.

As mentioned in the Section 2, an accelerated test procedure was carried out to evaluate catalyst stability under potential cycling conditions. Fig. 5 shows an example of accelerated degradation test for Pt/CNF650. All the electrodes followed the same trend. It can be observed how the oxygen reduction peak shifts to higher potentials and decreases in intensity during the cycling process, which can be attributed to an increase of particle size with a consequent reduction of the electrochemically surface area (ECSA) and increase of intrinsic catalytic activity for oxygen reduction, as already described in a previous work [39]. The cyclic voltammetry profiles are reported in Fig. 6 for the same electrode (Pt/CNF650) before and after the potential cycling procedure. It is clear from the hydrogen adsorption region (shaded area) that the ECSA decreases after the accelerated test, due to sintering or dissolution of Pt particles [39–41].

Fig. 7 shows the electrochemically active surface areas (ECSA) for the electrocatalysts, before and after the degradation procedures. The ECSA values show a maximum for the Pt/CNF650 due to its best compromise in terms of support surface area and dispersion as resulting from a moderate concentration of surface groups in the

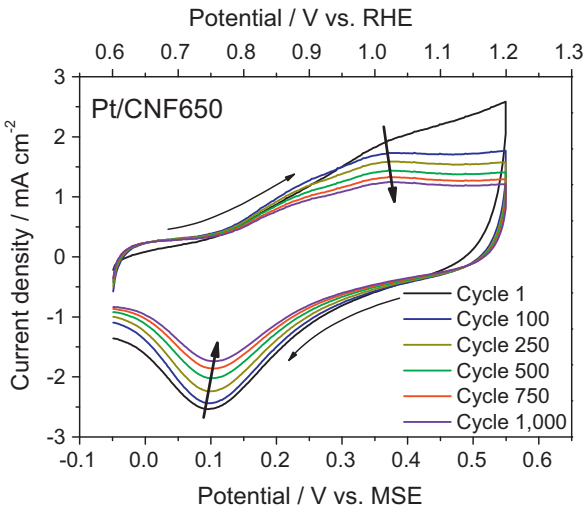

Fig. 5. Accelerated Pt degradation test by potential cycling for Pt/CNF650, 1000 cycles in 0.5 M H_2SO_4 at room temperature.

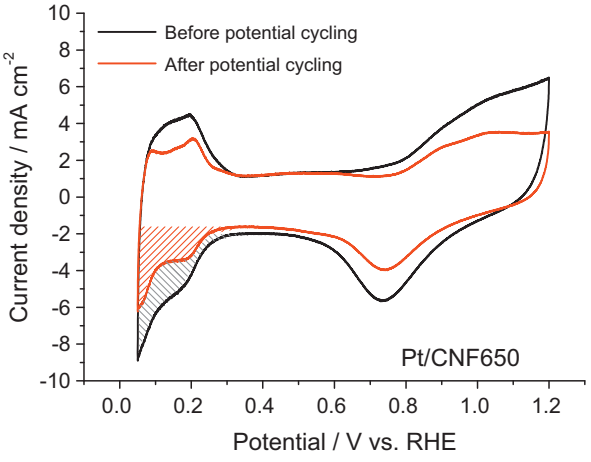

Fig. 6. Cyclic voltammetry for Pt/CNF650 electrode before and after Pt degradation test (20 mV s^{-1}, 0.5 M H_2SO_4, room temperature). The shaded area indicates the hydrogen adsorption region for the calculation of the electrochemically active surface area before (▨) and after (▨) the potential cycling.

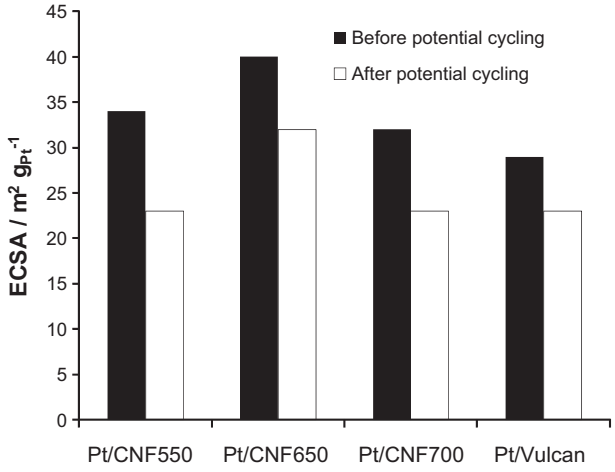

Fig. 7. Electrochemically active surface areas (ECSA) for the electrodes before and after Pt degradation tests.

support as discussed above. The effect of metal–support interaction significantly reduces the ECSA in the Pt/Vulcan catalyst with respect to the theoretical surface area derived from the mean crystallite size [42].

After the degradation tests, the relative decrease of ECSA is the highest for the sample based on the CNF synthesized at 550 °C. This is indeed the sample with the highest degree of agglomeration and includes a significant amount of particles which are not anchored on the support (see TEM micrograph). The sample based on the CNF synthesized at 650 °C is characterized by suitable BET surface area of the support allowing a proper anchoring effect and optimized dispersion that reduces the number of agglomerates where the corrosion effect (dissolution and reprecipitation) is more dramatic. This sample (CNF650) shows the lowest decrease of ECSA among the CNF-based catalysts. The decay of ECSA after accelerated tests increased in the sample based on the support synthesized at 700 °C because of the decrease of BET area with consequent lower contribution of the support in stabilizing the Pt particles through a metal–support interaction. The metal–support interaction [42] instead appears to play an effective role for Vulcan which has a relevant content of surface groups with respect to the CNFs. The decrease of ECSA for Vulcan is similar to that of the sample based on the CNF synthesized at 650 °C despite the larger number of anchoring surface groups. In this regard, it is worth to mention that the decay of the ECSA is the result of two contributions, i.e. the Pt dissolution and reprecipitation and the carbon corrosion, resulting into oxidation to CO_2 [16,39–41]. Amorphous-like regions, which are occurring more frequently on the Vulcan (Fig. 4), may influence the overall behavior. Thus, there are two competing effects in the carbon black based catalyst, i.e., the anchoring effect of surface groups but also the poor stability of amorphous regions with respect to electrochemical carbon corrosion. The CNF650 is characterized by lower metal–support interaction with respect to Vulcan but it is also less prompt to electrochemical carbon corrosion being essentially graphitic (see Table 1).

The effect of potential cycling on the electrocatalytic activity towards oxygen reduction reaction (ORR) in half-cell is illustrated in Fig. 8 for the Pt/CNF650 and the mass activity for all the samples is reported in Fig. 9. The mass activity before the accelerated test is the largest on the sample Pt/CNF650 that has the highest ECSA; yet, if one analyses the trend for all samples in Fig. 9 in comparison to Fig. 7, it appears that there is no direct relationship between ECSA and mass activity and more precisely, the ECSA is not the key parameter determining the electrocatalytic activity for ORR. Very low mass activity is recorded for Pt/Vulcan and Pt/CNF550

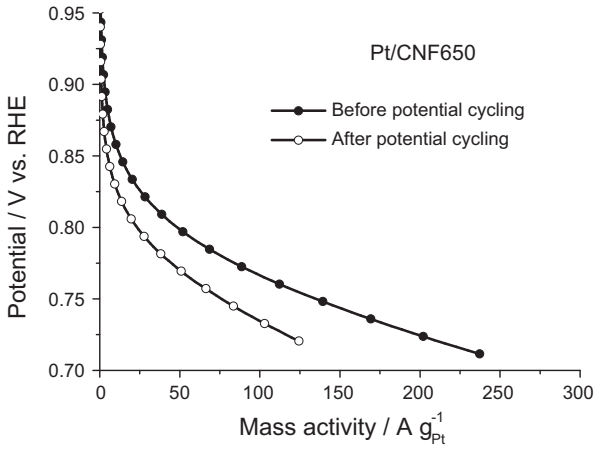

Fig. 8. Polarization curve for the oxygen reduction reaction in half-cell for Pt/CNF650 before and after Pt degradation test (pure oxygen, 0.5 M H_2SO_4, room temperature).

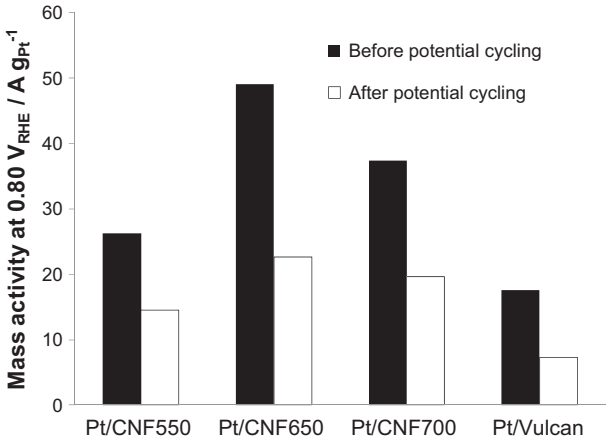

Fig. 9. Mass activity for the different electrocatalysts in ORR before and after Pt degradation from polarization curves at 0.80 V vs. RHE (pure oxygen, 0.5 M H_2SO_4, room temperature).

which are essentially the samples characterized by a large number of support surface groups/defects. In general, the number of surface groups is prevailing in the carbon black with respect to CNFs [43,44]. It is well known that the surface functional groups interact with Pt nanoparticles modifying the electronic environment of Pt sites available for oxygen chemisorption [42]. As shown in the literature, the lowest number of surface groups provides the best results in terms of intrinsic activity for oxygen reduction [42,45]. In this regard, Pt/Vulcan appears less appropriate than Pt/CNF.

The decrease of mass activity after the accelerated tests appears to mainly reflect the decrease of the ECSA for most of the samples. However, it is noted that the decreased mass activity is comparatively lower for the sample based on the CNF synthesized at 700 °C than that synthesized at 650 °C. This may be interpreted on the basis of the largest degree of graphitic character for the sample Pt/CNF700 (Table 1) which plays a stabilizing role on the Pt electronic characteristics and reduces degradation of catalytic activity.

4. Conclusions

Three different carbon nanofibers, varying in terms of average diameter, ordering degree and surface structure, were prepared and investigated as platinum support for the cathodic oxygen reduction reaction of polymer electrolyte fuel cells. The catalysts based on CNF supports with a larger degree of graphitic character and suitable BET surface area showed a reduced degradation of catalytic activity after accelerated tests compared to Vulcan and high surface area CNF (550 °C) based catalysts. The Pt/CNF650 showed the highest ECSA values due to its best compromise in terms of support surface area and dispersion as resulting from a moderate concentration of surface groups in the support. The highest performance was obtained both before and after the accelerated degradation tests for the sample supported on CNF650 characterized by the highest ECSA and proper graphitic character of the support.

Acknowledgments

The authors wish to thank FEDER and the Spanish MICINN for financial support to project CTQ2011-28913-C02-01. The authors acknowledge the support of bilateral CNR (Italy)–CSIC (Spain) joint agreement 2011–2012 (project Baglio/Lazaro 2010IT0026).

References

[1] H. Liu, C. Song, L. Zhang, J. Zhang, H. Wang, D.P. Wilkinson, J. Power Sources 155 (2006) 95–110.
[2] S. Song, P. Tsiakaras, Appl. Catal. B 63 (2006) 187–193.
[3] S. Basri, S.K. Kamarudin, W.R.W. Daud, Z. Yaakub, Int. J. Hydrogen Energy 35 (2010) 7957–7970.
[4] V. Baglio, A. Stassi, F.V. Matera, V. Antonucci, A.S. Aricò, Electrochim. Acta 54 (2009) 2004–2009.
[5] C. D'Urso, V. Baglio, V. Antonucci, A.S. Aricò, S. Specchia, U.A. Icardi, G. Saracco, C. Spinella, G. D'Arrigo, Int. J. Hydrogen Energy 36 (2011) 8088–8093.
[6] S. Song, Y. Liang, Z. Li, Y. Wang, R. Fu, D. Wu, P. Tsiakaras, Appl. Catal. B 98 (2010) 132–137.
[7] F. Kadirgan, A.M. Kannan, T. Atilan, S. Beyhan, S.S. Ozenler, S. Suzer, A. Yörür, Int. J. Hydrogen Energy 34 (2009) 9450–9460.
[8] E. Antolini, T. Lopes, E.R. Gonzalez, J. Alloys Compd. 461 (2008) 253–262.
[9] V. Baglio, A. Stassi, A. Di Blasi, C. D'Urso, V. Antonucci, A.S. Aricò, Electrochim. Acta 53 (2007) 1360–1364.
[10] A. Stassi, C. D'Urso, V. Baglio, A. Di Blasi, V. Antonucci, A.S. Aricò, A.M. Castro Luna, A. Bonesi, W.E. Triaca, J. Appl. Electrochem. 36 (2006) 1143–1149.
[11] S. Sari Ozenler, F. Kadirgan, J. Power Sources 154 (2006) 364–369.
[12] E. Antolini, J.R.C. Salgado, L.G.R.A. Santos, G. Garcia, E.A. Ticianelli, E. Pastor, E.R. Gonzalez, J. Appl. Electrochem. 36 (2006) 355–362.
[13] R.C. Koffi, C. Coutanceau, E. Garnier, J.-M. Leger, C. Lamy, Electrochim. Acta 50 (2005) 4117–4127.
[14] S. Song, Y. Wang, P. Tsiakaras, P.K. Shen, Appl. Catal. B 78 (2008) 381–387.
[15] T. Kottakkat, A.K. Sahu, S.D. Bhat, P. Sethuraman, S. Parthasarathi, Appl. Catal. B 110 (2011) 178–185.
[16] R. Borup, J. Meyers, B. Pivovar, Y.S. Kim, R. Mukundan, N. Garland, D. Meyers, M. Wilson, F. Garzon, D. Wood, P. Zelenay, K. More, K. Stroh, T. Zawodzinski, J. Boncella, J.E. McGrath, M. Inaba, K. Miyatake, M. Hori, K. Ota, Z. Ogumi, S. Miyata, A. Nishikata, Z. Siroma, Y. Uchimoto, K. Yasuda, K. Kimijima, N. Iwashita, Chem. Rev. 107 (2007) 3904–3951.
[17] W. Schmittinger, A. Vahidi, J. Power Sources 180 (2008) 1–14.
[18] Y. Shao, G. Yin, Y. Gao, J. Power Sources 171 (2007) 558–566.
[19] J. Wu, X.Z. Yuan, J.J. Martin, H. Wang, J. Zhang, J. Shen, S. Wu, W. Merida, J. Power Sources 184 (2008) 104–119.
[20] S. Zhang, X.Z. Yuan, J.N.C. Hin, H. Wang, K.A. Friedrich, M. Schulze, J. Power Sources 194 (2009) 588–600.
[21] Z. Siroma, K. Ishii, K. Yasuda, Y. Miyazaki, M. Inaba, A. Tasaka, Electrochem. Commun. 7 (2005) 1153–1156.
[22] M. Cai, M.S. Ruthkosky, B. Merzougui, S. Swathirajan, M.P. Balogh, S.H. Oh, J. Power Sources 160 (2006) 977–986.
[23] H.A. Gasteiger, S.S. Kocha, B. Sompalli, F.T. Wagner, Appl. Catal. B 56 (2005) 9–35.
[24] Y. Shao, G. Yin, J. Zhang, Y. Gao, Electrochim. Acta 51 (2006) 5853–5857.
[25] X. Yu, S. Ye, J. Power Sources 172 (2007) 145–154.
[26] E. Antolini, Appl. Catal. B 88 (2009) 1–24.
[27] Y. Ma, S. Jiang, G. Jian, H. Tao, L. Yu, X. Wang, X. Wang, J. Zhu, Z. Hu, Y. Chen, Energy Environ. Sci. 2 (2009) 224–229.
[28] D. Morales-Acosta, J. Ledesma-Garcia, Luis A. Godinez, H.G. Rodríguez, L. Álvarez-Contreras, L.G. Arriaga, J. Power Sources 195 (2010) 461–465.
[29] V. Baglio, A. Di Blasi, C. D'Urso, V. Antonucci, A.S. Aricò, R. Ornelas, D. Morales-Acosta, J. Ledesma-Garcia, L.A. Godinez, L.G. Arriaga, L. Alvarez-Contreras, J. Electrochem. Soc. 155 (2008) B829–B833.
[30] M.J. Lázaro, D. Sebastián, I. Suelves, R. Moliner, J. Nanosci. Nanotechnol. 9 (2009) 4353–4359.
[31] D. Sebastián, I. Suelves, M.J. Lázaro, R. Moliner, J. Power Sources 192 (2009) 51–56.
[32] S. Eriksson, U. Nylén, S. Rojas, M. Boutonnet, Appl. Catal. A 265 (2004) 207–219.
[33] D. Sebastián, M.J. Lázaro, I. Suelves, R. Moliner, V. Baglio, A. Stassi, A.S. Aricò, Int. J. Hydrogen Energy (2011), doi:10.1016/j.ijhydene.2011.07.004.
[34] D. Sebastián, I. Suelves, R. Moliner, M.J. Lázaro, Carbon 48 (2010) 4421–4431.
[35] V. Baglio, A. Di Blasi, A.S. Aricò, V. Antonucci, P.L. Antonucci, F. Nannetti, V. Tricoli, Electrochim. Acta 50 (2005) 5181–5188.
[36] T. Denaro, V. Baglio, M. Girolamo, V. Antonucci, A.S. Aricò, F. Matteucci, R. Ornelas, J. Appl. Electrochem. 39 (2009) 2173–2179.
[37] S. Maass, F. Finsterwalder, G. Frank, R. Hartmann, C. Merten, J. Power Sources 176 (2008) 444–451.
[38] K. Kinoshita, J. Bett, Carbon 11 (1973) 237–247.
[39] A.S. Aricò, A. Stassi, E. Modica, R. Ornelas, I. Gatto, E. Passalacqua, V. Antonucci, J. Power Sources 178 (2008) 525–536.
[40] A.S. Aricò, A. Stassi, I. Gatto, G. Monforte, E. Passalacqua, V. Antonucci, J. Phys. Chem. C 114 (2010) 15823–15836.
[41] A. Stassi, E. Modica, V. Antonucci, A.S. Aricò, Fuel Cells 3 (2009) 201–208.
[42] A.S. Aricò, P.L. Antonucci, V. Antonucci, in: A. Wieckowski, E.R. Savinova, C.G. Vayenas (Eds.), Catalysis and Electrocatalysis at Nanoparticle Surfaces, Marcel Dekker, Inc., New York, 2003, p. 613.
[43] A.S. Aricò, V. Antonucci, M. Minutoli, N. Giordano, Carbon 27 (1989) 337–347.
[44] A.S. Aricò, V. Antonucci, L. Pino, P.L. Antonucci, N. Giordano, Carbon 28 (1990) 599–609.
[45] N. Giordano, P.L. Antonucci, E. Passalacqua, L. Pino, A.S. Aricò, K. Kinoshita, Electrochim. Acta 36 (1991) 1931–1935.